analytical chemistry

pubs.acs.org/ac Article

Biomimetic Chip Enhanced Time-Gated Luminescent CRISPR-Cas12a Biosensors under Functional DNA Regulation

Cheng-Yu Li,*,# Bei Zheng,# Li-Li Lu,# Wen-Kai Fang, Ming-Qiu Zheng, Jia-Ling Gao, Liu Yuheng, Dai-Wen Pang, and Hong-Wu Tang*

Cite This: *Anal. Chem.* 2021, 93, 12514−12523 Read Online

ACCESS | Metrics & More | Article Recommendations | Supporting Information

ABSTRACT: Despite that the currently discovered CRISPR-Cas12a system is beneficial for improving the detection accuracy and design flexibility of luminescent biosensors, there are still challenges to extend target species and strengthen adaptability in complicated biological media. To conquer these obstacles, we present here some useful strategies. For the former, the limitation to nucleic acids assay is broken through by introducing a simple functional DNA regulation pathway to activate the unique trans-cleavage effect of this CRISPR system, under which the expected biosensors are capable of effectively transducing a protein (employing dual aptamers) and a metal ion (employing DNAzyme). For the latter, a time-gated luminescence resonance energy transfer imaging manner using a long-persistent nanophosphor as the energy donor is performed to completely eliminate the background interference and a nature-inspired biomimetic periodic chip constructed by photonic crystals is further combined to enhance the persistent luminescence. In line with the above efforts, the improved CRISPR-Cas12a luminescent biosensor not only exhibits a sound analysis performance toward the model targets (carcinoembryonic antigen and Na^+) but also owns a strong anti-interference feature to actualize accurate sensing in human plasma samples, offering a new and applicative analytical tool for laboratory medicine.

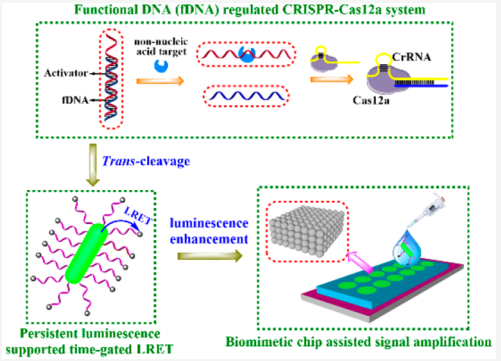

The occurrence and progression of diseases are generally related to the excess, lack, and abnormal function of biomolecules in human body fluids such as blood, urine, and saliva.[1,2] Thus, developing efficient analytical technologies for disease-associated biomarkers plays a crucial role in clinical recognition and treatment. Until now, thanks to the effective target transduction pathway and the convenient signal output mode, the biosensing-based assay means have attracted widespread attention.[3,4] Although much effort in improving sensitivity has been made to this sound choice, there is still a challenge to further strengthen its detection accuracy.

In recent years, a vitally innovative genome-editing method concentrated on the clustered regularly interspaced short palindromic repeats (CRISPR) is promising for fulfilling this goal. The inspiration of this "genetic scissor" comes from the adaptive immune defense system produced by the evolutionary struggle between bacteria and virus.[5] Principally, a sequence of guided RNA (termed as CrRNA) is first combined with a Cas endonuclease to form a Cas/CrRNA complex, and then the target nucleic acid will be degraded when it directionally complements to the CrRNA. With the assistance of such a rigorous base-pairing reliant cleavage standard, the further integration of CRISPR into various biosensing platforms including colorimetry,[6−9] electrochemistry,[10−12] and luminescence[13−18] is capable of significantly promoting the transduction accuracy. In contrast to the broadly used CRISPR-Cas9 system, another newly found type V enzyme (Cas12a) is not only able to implement the routine cleavage toward a complementary target (referred to as cis-cleavage) but also possesses a special cleavage capability for indiscriminately degrading an additional nontarget single-stranded DNA (referred to as trans-cleavage).[19,20] Taking advantage of this collateral effect, the design of CRISPR-mediated biosensors (especially luminescent biosensors) will be more flexible. However, the existing luminescent CRISPR-Cas12a biosensors continue to suffer from the following bottlenecks.

For one thing, due to the deficiency of adequate transduction patterns to activate the Cas12a effector, most of the reported biosensors are only able to satisfy the requirement of detecting nucleic acid molecules, and such a limited application range has severely hampered their progress. To extend the variety of sensing targets, Liang et al.[14] incorporated bacterial allosteric transcription factors (aTFs) into the CRISPR-Cas12a system and realized the analysis of non-nucleic acid targets,

Received: April 1, 2021
Published: September 7, 2021

https://doi.org/10.1021/acs.analchem.1c01403
Anal. Chem. 2021, 93, 12514−12523

Scheme 1. Schematic Diagram and Workflow of the Biomimetic Chip Enhanced Time-Gated Luminescent CRISPR-Cas12a Biosensor by Making Use of a Functional DNA Regulation Pathway to Transduce Non-nucleic Acid Targets[a]

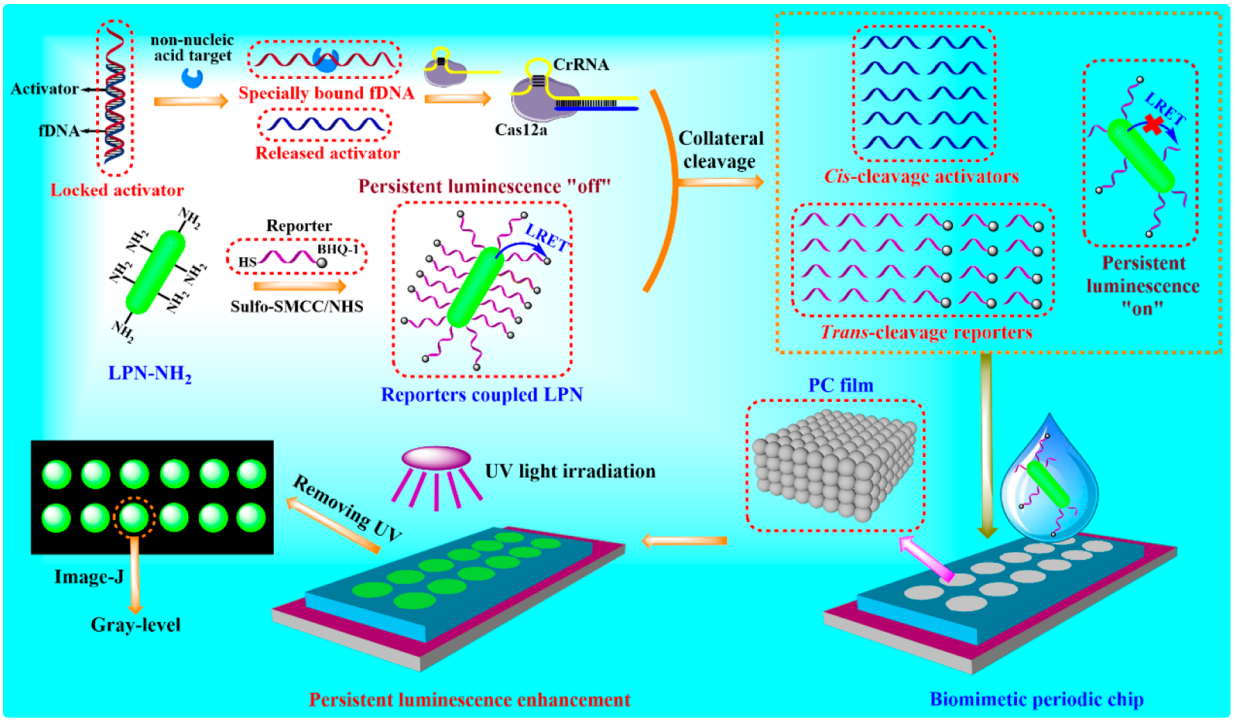

[a]The objects are not drawn in real scale.

although this concept is suitable for a few kinds of small molecules because of the restricted recognition scopes of aTFs. Comparatively, the introduction of functional DNA with a wider target binding ability (from small molecules to biomacromolecules) can well-resolve this drawback.[16]

For another, the acquisition of optical signals for these luminescent biosensors is mostly focused on the commonly applied Stokes emission by selecting a source within visible light, forcing a poor capacity to avoid the interference of background signals in complicated biological media such as human plasma.[21,22] Although our previous work[23] has employed a kind of anti-Stokes luminescence mode (upconversion luminescence) to partly address this concern, the complex synthesis process (a high-temperature thermal decomposition based seed-mediated growth) of the upconversion nanoparticle and the harsh nonlinear multiphoton absorption behavior under a very high photodensity condition compel it to be short of user friendliness. Inspiringly, another option, which is the long-persistent nanophosphor (LPN), can perfectly conquer these problems. An LPN is a type of luminophore that can maintain the luminescence phenomenon after removing the excitation source [normally a simple and moderate ultraviolet (UV) light], and such a persistent feature normally sustains from a few minutes to several days.[24−28] Theoretically, because the luminescence lifetimes of diverse matrixes in biological samples are basically in the nanosecond regime, this short-lived background window can be effectively eliminated by utilizing the LPN-supported luminescence detection. To the best of our knowledge, the introduction of such a time-gated imaging manner into luminescent CRISPR-Cas12a biosensors has not been reported yet.

In spite of the fact that the use of an LPN is a good proposal for reinforcing the working adaptation to face with complicated samples, the sharp decay of persistent luminescence is also a potential issue. As is well-known, the luminescence intensity can directly determine the sensing sensitivity, and thus, exploring a strategy to enhance the attenuated luminescence signals is a key point. Encouragingly, a wealth of structural materials in nature offer a useful guidance. A typical case is the strong reflection of sunlight by the Morpho butterfly; such an interesting natural phenomenon derives from the periodic arrangement of flakes in its wings.[29] Following this hint, similar microstructures are endowed to many artificial materials to achieve the selective transmission of light, of which a periodic biomimetic structure formed by the self-assembly of nanospheres (termed a photonic crystal) has paved an alternative venue in the field of solid-phase chips, and this regular three-dimensional interface is a hopeful approach for compensating and even amplifying the signals of persistent luminescence;[30−33] such solving means has not been employed in other time-gated luminescence sensing work.

On the basis of the above motivations, a new time-gated CRISPR-Cas12a biosensor is put forward here by integrating a functional DNA (denoted as fDNA) regulation pathway with a photonic crystal (denoted as PC) chip triggered luminescence enhancement, and it is exploited to implement the accurate and sensitive transduction of non-nucleic acid targets (e.g., proteins and metal ions). The schematic diagram and workflow of this sensing method are illustrated in detail in Scheme 1. On one hand, a locking process is actualized to an activator which completely complements to the right end of the hairpin structure of CrRNA by hybridizing with part of the fDNA. In the presence of a non-nucleic acid target, owing to the higher affinity of fDNA than the rationally designed binding force of base pairing, the hybridization structure is dissociated, and the released activator will effectively identify a free Cas12a/

https://doi.org/10.1021/acs.analchem.1c01403
Anal. Chem. 2021, 93, 12514−12523

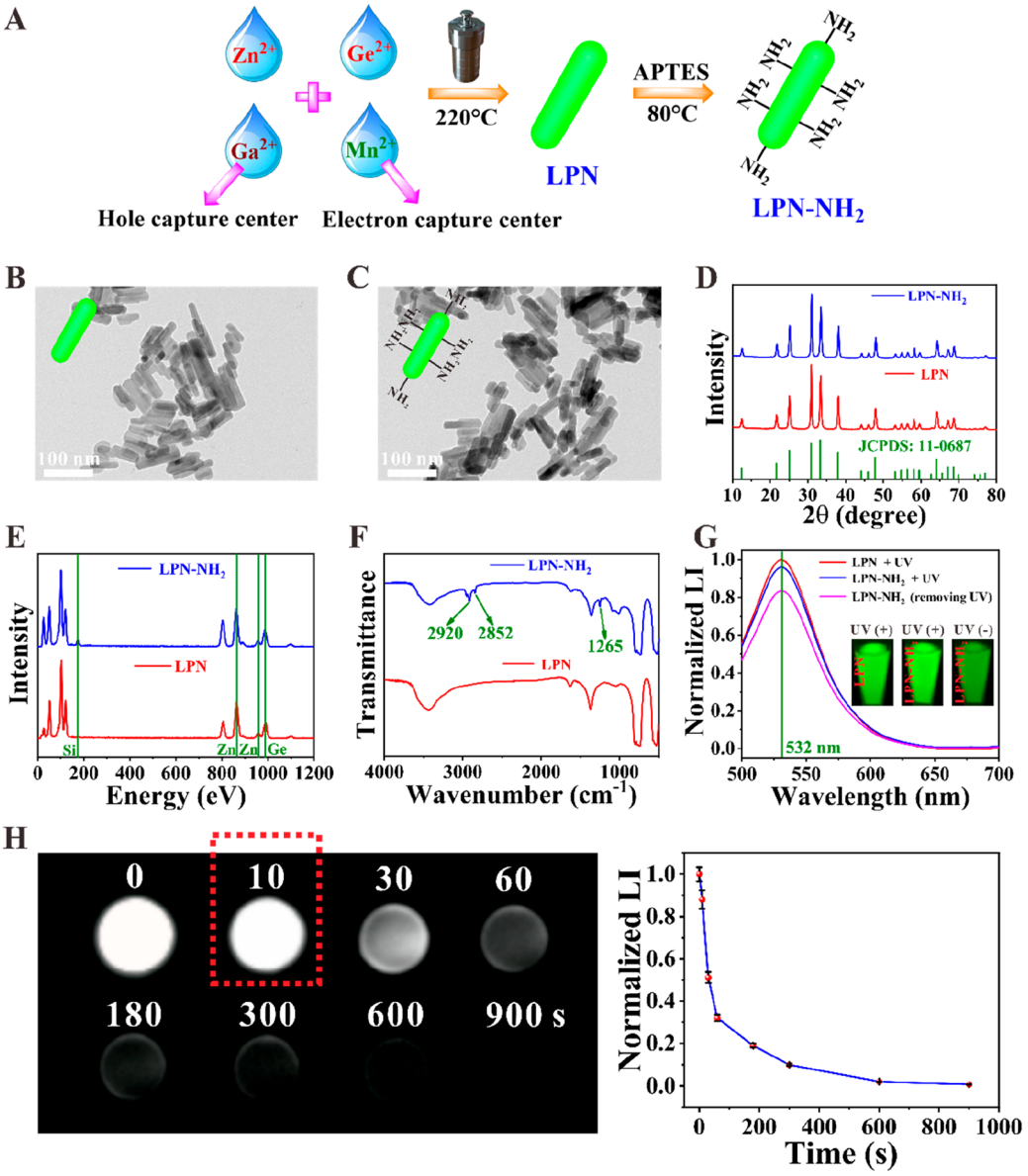

Figure 1. (A) Synthetic route and water-soluble functionalization of the LPN. The objects are not drawn in real scale. (B) TEM image of the LPN. The scale bar is 100 nm. (C) TEM image of the LPN−NH_2. The scale bar is 100 nm. (D) XRD patterns of the LPN and LPN−NH_2. (E) EDS lines of the LPN and LPN−NH_2. (F) FT-IR spectra of the LPN and LPN−NH_2. (G) Red and blue lines: luminescence spectra of the LPN and LPN−NH_2 solutions under the illumination of a 365 nm UV lamp. Purple line: luminescence spectrum of the LPN−NH_2 solution after immediately removing the UV lamp. Inset: real digital images of the corresponding solutions presented in the luminescence spectra. (H) Long-lifetime luminescence test for the LPN−NH_2 solution after removing the 365 nm UV source for 15 min. Left: real luminescence images with time evolution. The red dotted box indicates the time node (10 s) of the luminescence acquisition. Right: the corresponding luminescence attenuation curve.

CrRNA complex. On the other hand, a double modified DNA strand (sulfhydryl and BHQ-1 at both ends, denoted as the reporter) with a very short length (only 5 nt) is covalently coupled onto the surface of an amino groups functionalized LPN (denoted as LPN−NH_2). For the as-prepared reporters-coupled LPN, a dramatic quenching effect toward the persistent luminescence can be produced due to the luminescence resonance energy transfer (LRET) between the proximate LPN−NH_2 (energy donor) and the BHQ-1 molecule (energy receptor). When the collateral cleavage of the CRISPR-Cas12a system is activated, both the activator and the reporters will be degraded into fragments. In this case, a signal recovery phenomenon is presented to the as-quenched persistent luminescence. For the next quantitative analysis, the as-cleaved products are loaded onto the PC film of a biomimetic periodic chip, and a time-gated imaging (after removing the excitation source) determined by gray-levels using an ImageJ software and a complementary metal oxide semiconductor (CMOS) camera equipped commercial device is finally performed under the irradiation of a 365 nm UV lamp.

EXPERIMENTAL SECTION

Synthesis of the LPN. First, 0.985 mmol of GeO_2 powder was fully mixed together with 2 M NaOH solution in a 50 mL beaker for at least 10 min to form a homogeneous solution.

https://doi.org/10.1021/acs.analchem.1c01403
Anal. Chem. 2021, 93, 12514−12523

Then, the as-obtained Na_2GeO_3 solution was added dropwise into a mixture solution containing 300 μL of concentrated HNO_3, 2 mmol of $Zn(NO_3)_2{\cdot}6H_2O$, 0.01 mmol of $Ga(NO_3)_3{\cdot}xH_2O$, 0.005 mmol of $Mn(NO_3)_2{\cdot}6H_2O$, and 11 mL of deionized water. After adjusting the pH value of the above solution to 9.5 by providing a certain amount of ammonium hydroxide drop by drop, the mixture was kept stirring vigorously at room temperature for 60 min, followed by transferring to a 25 mL Teflon-lined autoclave. Subsequently, the autoclave was quickly heated to 220 °C within 15 min and maintained warm for 8 h under gentle stirring. Once cooled to room temperature, the precipitates were collected by centrifuging at 8000 rpm for 5 min and washed several times with deionized water. Finally, ultrasonic treatment was performed to the resulting products in 4 mL of deionized water for 10 min to regulate the concentration at ∼20 mg/mL.

Synthesis of the LPN−NH_2. An amount of 50 mg of the as-synthesized LPN was first stirred vigorously with 20 mL of *N*,*N*-dimethylformamide in a 50 mL round-bottom flask for at least 10 min, and then the mixture solution was heated to 80 °C, followed by carefully dropping 200 μL of 3-aminopropyltriethoxysilane (APTES). After maintaining the warmth for 6 h, the cooled precipitates were collected by centrifugation and washed three times with deionized water. Finally, the resulting products were redispersed into 2 mL of deionized water via ultrasonic treatment (concentration ∼20 mg/mL) and kept at 4 °C for a long time.

Preparation of the Reporters-Coupled LPN. An amount of 10 μL of the as-synthesized LPN−NH_2 solution was first added into a 2 mL tube containing 100 μL of 4-(2-hydroxyethyl)piperazine-1-ethanesulfonic acid (HEPES) buffer solution (20 mM, pH 7.4), and then the mixture was treated with a vortex for at least 5 min, followed by introduction of a freshly prepared mixture solution by dissolving with 0.8 mg of 4-(*N*-maleimidomethyl)cyclohexane-1-carboxylic acid 3-sulfo-*N*-hydroxysuccinimide ester sodium salt (sulfo-SMCC) and 0.8 mg of *N*-hydroxysuccinimide (NHS). After fully mixing together with 10 nmol of reporter and transferring to a thermostatic oscillator, the tube was allowed to incubate gently at 37 °C for 60 min. Subsequently, a certain amount of extra sulfo-SMCC was supplied, and the incubation was continued for another 30 min. Next, centrifugal processing at 8000 rpm was conducted to dispose of the residual reporters, and the collected products were further washed four times with HEPES buffer solution containing 1% Tween-20. The final precipitates were redispersed into 50 μL of reaction buffer solution (30 mM Tris-base, 10 mM $MgCl_2$, 0.1 mg/mL BSA, pH 8.0) via ultrasonic treatment and stored at 4 °C for later use.

Fabrication of the Biomimetic Periodic Chip. First, a cover glass (22 × 50 × 0.17 mm) was washed in sequence with 3% hydrochloric acid, ethanol/acetone (v/v = 1:1), and deionized water via ultrasonic immersion for 30 min. Then, the as-cleaned cover glass was fully blown dry with a high-purity Ar flow and soaked overnight in a sealed watch glass (90 mm) containing 15 mL of APTES. Next, the as-silanized cover glass was coated with a layer (thickness ∼3 mm) of poly(dimethylsiloxane) (PDMS) film in a high-vacuum and dust-free oven at 60 °C. Thereafter, the PDMS film was uniformly punched with 12 hollow holes (diameter ∼5 mm). Subsequently, to each hole a 10 μL droplet of 50 mg/mL deionized water washed polystyrene spheres (PS, size ∼240 nm) was carefully dropped. Finally, the as-treated cover glass was transferred to a drying oven and further put to rest at 37 °C for at least 3 h.

Combination of Cas12a and CrRNA (Cas12a/CrRNA Complex). Initially, 0.2 nmol of Lbcas12a dissolved in reaction buffer solution and 0.1 nmol CrRNA dissolved in diethyl pyrocarbonate treated water were fully mixed together in a 2 mL RNase-free tube through a vortex. Next, the tube was allowed to incubate gently at 37 °C for 15 min.

RESULTS AND DISCUSSION

Synthetic Route, Characterization, and Surface Covalent Coupling of the LPN. As presented in Figure 1A, a conventional hydrothermal method[34] at 220 °C using nitrate hydrates as the precursors is performed to create the surface-bared LPN (Zn_2GeO_4: Ga, Mn) by codoping 1% Ga^{2+} (acting as the hole capture center) and 0.5% Mn^{2+} (acting as the electron capture center) into a Zn_2GeO_4 host matrix. After that, the hydrophobic surface is functionalized with amino groups by grafting APTES molecules at 80 °C.

The morphology evolution of such a synthetic route is clearly exhibited in transmission electron microscopy (TEM) images (Figure 1, parts B and C), wherein the two nanoparticles are kept in regular rod shapes. Size statistical data (n = 300, Figure S1) reveal that the average length and width of the LPN are 63.08 and 14.51 nm, respectively, along with a negligible size fluctuation that appears to the hydrophilic ones (Figure S2), also indicating the favorable crystal maintenance during the surface change. The highly crystalline properties and the well-resolved lattice fringes (adjacent interplanar spacings ∼0.29 nm) displayed in high-resolution TEM images (Figure S3, parts A and B) collectively prove that the (113) faces in these rod directions are single crystals. This fact is further verified by X-ray diffraction (XRD) patterns (Figure 1D), among which no impurities arise to both cases, and their distinct positions of diffraction peaks are indistinguishably in consistence with the normative card of Zn_2GeO_4 (JCPDS: 11-0687). X-ray spectroscopy (EDS) lines (Figure 1E) uncover the defined distribution of primary metallic elements (Zn and Ge) in each nanorod, while a new location vested in the silicon element occurs in the LPN−NH_2. With the contributions of the −CH_2− stretching bands (2920 and 2852 cm^{-1}) and the assignment of the Si−O−Si vibration (1265 cm^{-1}) in the Fourier transform infrared (FT-IR) spectra (Figure 1F),[35] the surface grafting is finely manifested, and such water-soluble functionalization enables the formation of a transparent solution (Figure S3C).

Under the illumination of a 365 nm UV lamp, it is observed that the LPN solution emits bright green light, and the maximum emission peak is at around 532 nm (Figure 1G, red line and inset). Of note, the surface APTES molecules do not cause obvious attenuation to the green luminescence (Figure 1G, blue line). More interestingly, such featured emission can be maintained preferably after immediately removing the excitation source (Figure 1G, purple line and inset). To test the long-lifetime luminescence ability, the LPN−NH_2 solution is then loaded onto a 96-well plate and irradiated continuously for 10 min to make the hole capture center (Ga^{2+}) fully store the excitation energy. In Figure 1H, the gray-levels of persistent luminescence are able to be captured even in the absence of the UV lamp for as long as 15 min through our imaging device, rendering a satisfactory optical duration window to avoid the background interference resulting from biological media. Considering the demand of sufficient

https://doi.org/10.1021/acs.analchem.1c01403
Anal. Chem. 2021, 93, 12514−12523

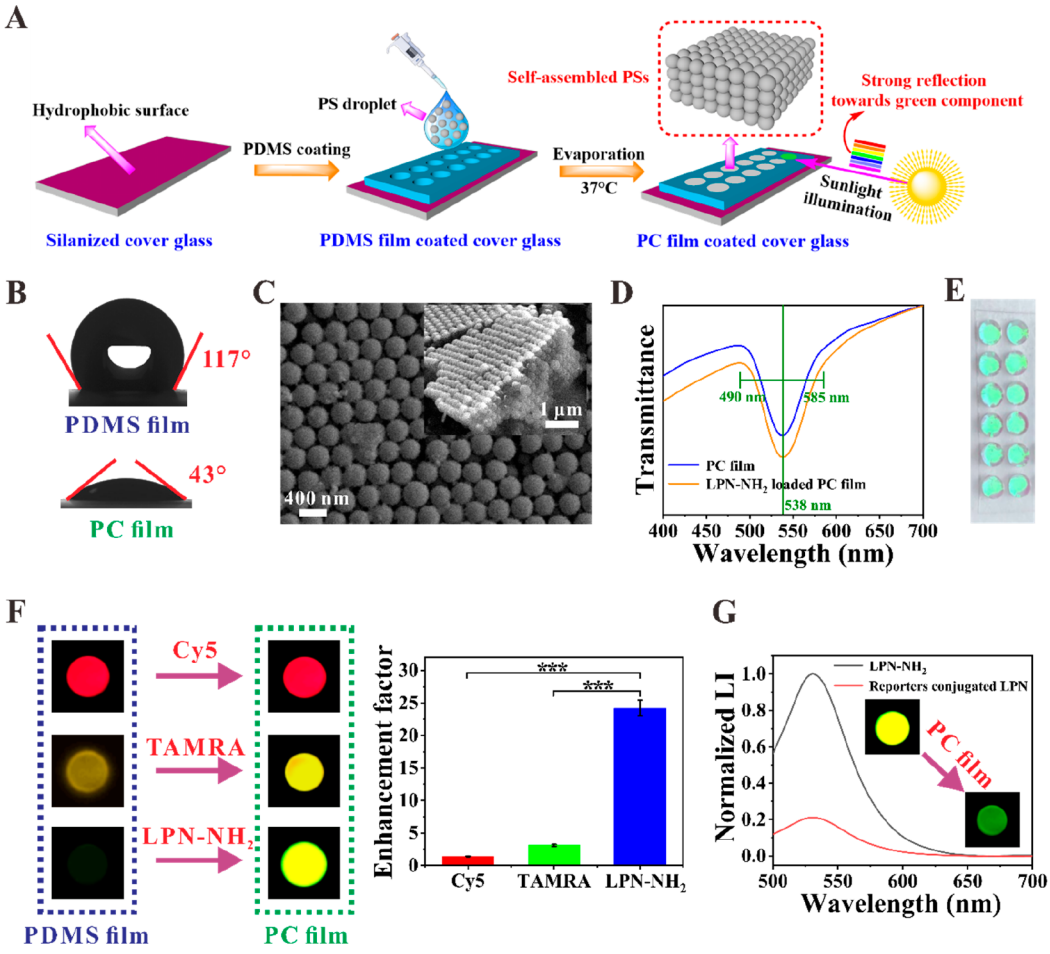

Figure 2. (A) Fabrication steps of the self-made biomimetic periodic chip. The objects are not drawn in real scale. (B) Contact angle measurements of the PDMS and PC films. (C) SEM image of the PC film in the horizontal direction. The scale bar is 400 nm. Inset: SEM image (scale bar is 1 μm) of the PC film in the vertical direction. (D) Transmittance spectra of the PC film and LPN−NH_2-loaded PC film. (E) Real digital image of the biomimetic periodic chip under the illumination of sunlight. (F) Left: luminescence images (false-color) of Cy5-, TAMRA-, and LPN−NH_2-loaded PDMS and PC films under the optimal excitation sources, respectively. Right: enhancement factor of the PC film to Cy5, TAMRA, and LPN−NH_2. ***P < 0.001. (G) Quenching effect of BHQ-1 toward persistent luminescence in a homogeneous solution (luminescence spectra) and on the PC film (luminescence images).

detection signals, we select 10 s of decay as the time node of the luminescence acquisition.

After coupling the amino sites of the LPN−NH_2 with the sulfhydryl end of the reporter through sulfo-SMCC/NHS chemistry, it can be found that the ζ-potentials turn negative (from +11.8 mV to −10.2 mV, Figure S4A) and the hydrate particle sizes show a slight increase (Figure S4B). In addition, the complete disappearance of spectral absorbance at approximately 260 nm (a characteristic indicator for nucleic acid molecules,[36] Figure S5A) for the centrifugal supernatant visibly demonstrates a highly efficient covalent binding event, and the attached DNA molecules will not separate away from the LPN surface (Figure S5B). By further approximating the LPN−NH_2 as a standard cylinder (the detailed calculation process is shown in the Supporting Information), it can be evaluated that ∼274 reporters are coupled onto the surface of a single LPN−NH_2, and the luminescence intensity of the reporters-coupled LPN can keep favorable stability under the treatment of a high concentration of endogenous nuclease (Figure S6).

Fabrication Steps and Characterization of the Biomimetic Periodic Chip. The detailed fabrication steps of our self-made biomimetic periodic chip are shown in Figure 2A, in which a silanization processing is first carried out to a well-cleaned cover glass, and then a thin layer (thickness ∼3 mm) of PDMS film is adhered onto the as-obtained hydrophobic surface. After uniformly punching 12 hollow holes (diameter ∼5 mm) on the surface of the PDMS film, a droplet containing plenty of monodispersed carboxyl PS is carefully dropped into each hole and put the integrated chip to rest at 37 °C to naturally evaporate off the internal aqueous solutions. The above batteries of surface treatments are commendably validated by contact angle measurements (Figure 2B), from which the high angle (∼117°) of the PDMS film is sharply decreased to 43° when deposited with the PC film, suggesting that a final hydrophilic modification is achieved. The scanning electron microscopy (SEM) image in the horizontal direction (Figure 2C) evidently illustrates that an obvious self-assembly phenomenon happens to the as-evaporated PS, by which a compact periodic arrangement structure with an extremely high order is formed, and such a feature will not be affected after the solution incubation (Figure S7). Furthermore, a typical multilayer distribution is endowed to such assembled behavior in the vertical SEM

https://doi.org/10.1021/acs.analchem.1c01403
Anal. Chem. 2021, 93, 12514−12523

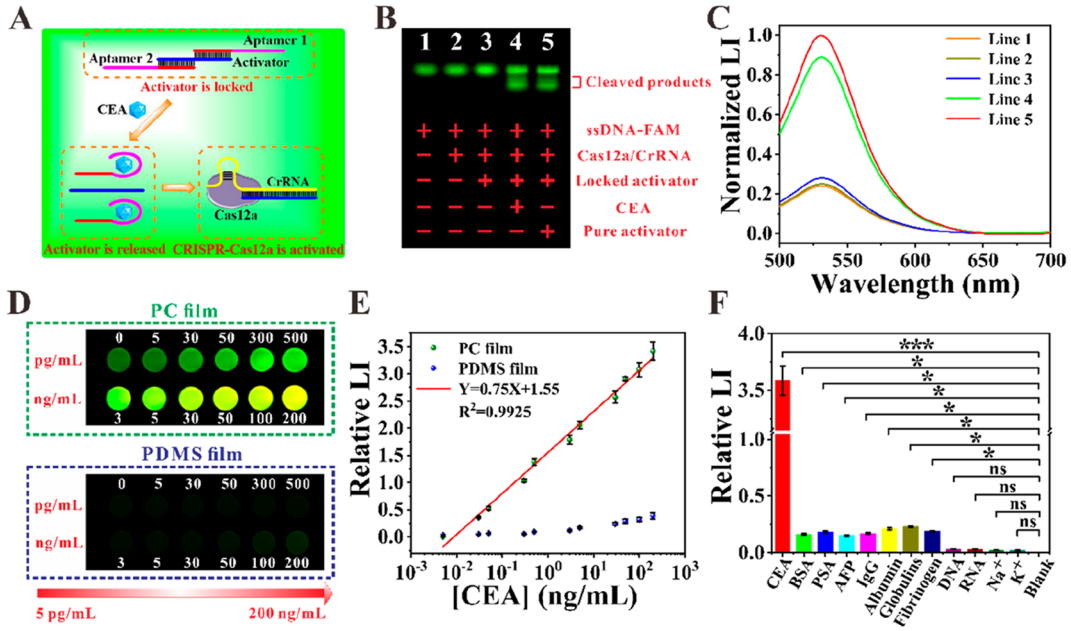

Figure 3. (A) Principle of the dual CEA aptamers-regulated CRISPR-Cas12a biosensor. The objects are not drawn in real scale. (B) A 1.5% agarose gel electrophoresis image of the proposed transduction pathway by trans-cleavage of ssDNA−FAM. Bands 1−5: ssDNA−FAM, ssDNA−FAM + Cas12a/CrRNA, ssDNA−FAM + Cas12a/CrRNA + locked activator, ssDNA−FAM + Cas12a/CrRNA + locked activator + CEA, ssDNA−FAM + Cas12a/CrRNA + pure activator. (C) Persistent luminescence spectra of the proposed transduction pathway by the trans-cleavage reporters-coupled LPN. Lines 1−5: reporters-coupled LPN, Cas12a/CrRNA + reporters-coupled LPN, Cas12a/CrRNA + reporters-coupled LPN + locked activator, Cas12a/CrRNA + reporters-coupled LPN + locked activator + CEA, Cas12a/CrRNA + reporters-coupled LPN + pure activator. (D) Persistent luminescence images (false-color) on PDMS (bottom) and PC (top) films in the presence of different amounts of CEA (from 5 pg/mL to 200 ng/mL). (E) Investigation of the linear working curves between the relative luminescence intensity and the logarithm of [CEA] on PDMS and PC films, respectively. (F) Specificity of the CEA detection toward BSA, PSA, AFP, IgG, albumin, globulins, fibrinogen, DNA, RNA, Na^+, and K^+. Concentrations of these substances are 10-fold higher than that of CEA. ***$P < 0.001$; *$P < 0.05$; ns, no significant difference ($P > 0.05$).

image (Figure 2C, inset). The transmittance spectrum (Figure 2D, blue line) explicitly confirms that the photonic band gap is less than 100 nm (covering from 490 to 585 nm), and the lowest transmission point is assigned at 538 nm. Notably, the additional loading of the LPN−NH_2 will not impact this specific band gap (Figure 2D, orange line). Because of the Bragg scattering principle, such unique light selection capacity makes the resulting chip able to intensely reflect the green component of sunlight (Figure 2E).

Inspection of the Luminescence Enhancement and Quenching Effect on the PC Film. Prior to bringing forward the expected CRISPR-Cas12a biosensors, two crucial issues need to be roundly inspected. On one hand, although the as-fabricated portable chip owns an ideal solid phase to realize signal amplification, it is still necessary to determine the practical luminescence enhancement of the PC film to the LPN. For this purpose, two well-known small-molecule fluorescent dyes, Cy5 and TAMRA, are loaded severally onto the PDMS and PC films. By virtue of the faultless overlap between the photonic band gap and the emission of the LPN, the LPN−NH_2 group presents the most remarkable luminescence enhancement effect (Figure 2F). Corresponding quantitative results reveal that the accurate enhancement factor for the LPN can reach up to 24.2, whereas it is dramatically declined to 3.1 and 1.4 for TAMRA and Cy5, respectively. Beyond that, the tiny differences in luminescence intensities for the inter- and intrabatches of biomimetic periodic chips (Figure S8) can lay a forceful foundation for the subsequent luminescence acquisition. On the other hand, in view of the employment of a traditional "off-to-on" mode sensing design, the quenching effect of BHQ-1 molecules toward the persistent luminescence is another challenge. Fortunately, because the very short chain length of the reporter is capable of bringing the pairing energy of the donors and receptors into proximity, a relatively high LRET efficiency (~78.2%) can be triggered either in a homogeneous solution or on the PC film (Figure 2G), and the optimal molar concentration of the reporter (in the presence of 200 μg of LPN−NH_2) is chosen as 10 nmol (Figure S9).

Principle of the Dual-Aptamer-Regulated CRISPR-Cas12a Biosensor and Its Analysis Performance toward Standard Carcinoembryonic Antigen (CEA). Supported by the above conclusive evidence, we began to establish the luminescence-enhanced time-gated CRISPR-Cas12a biosensors for the transduction of non-nucleic targets by means of the fDNA-based regulation. Initially, a common structure-switching model was proposed by selecting the widely applied CEA aptamer[37] as the representative fDNA. The specific sensing principle is described in Figure 3A, for which an activator is first absolutely locked via a simple annealing operation by one-step hybridizing with the ends of two properly prolonged CEA aptamers. Owing to the fact that the binding forces of the formed double-chain zones are far below the affinities of the aptamers to the target (the optimal reaction conditions are presented in Figure S10), the dual aptamers have priority to recognize CEA, and the activator will release from the dissociated hybridization frame to combine freely with a Cas12a/CrRNA complex to finally activate the CRISPR-Cas12a system. The trans-cleavage effect of the designed "lock-to-activate" pathway is then certified synergistically by agarose

https://doi.org/10.1021/acs.analchem.1c01403
Anal. Chem. 2021, 93, 12514−12523

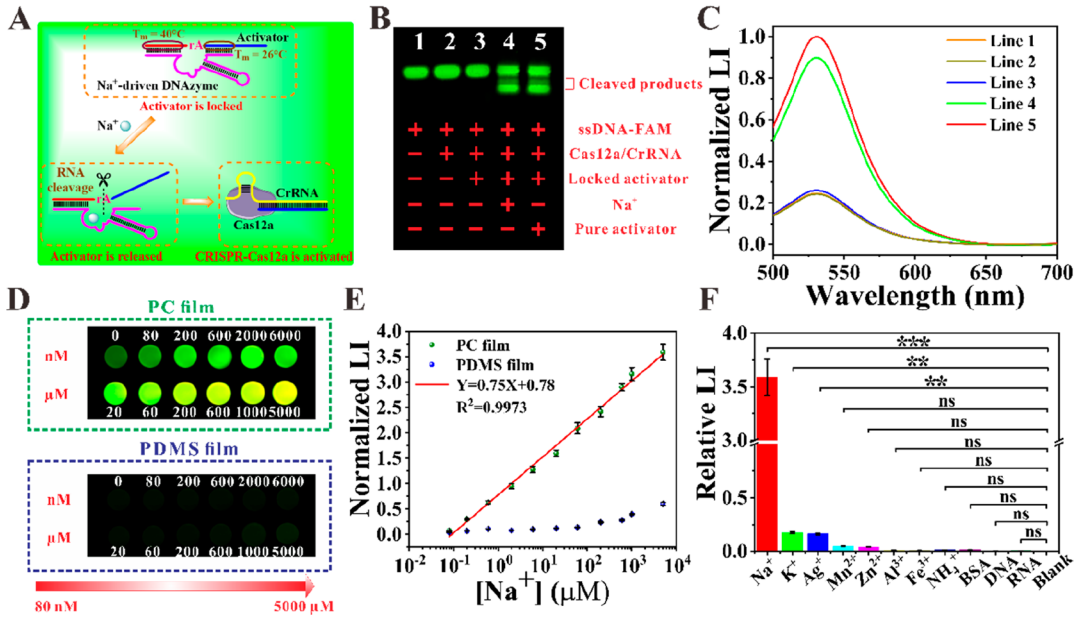

Figure 4. (A) Principle of the Na^+-driven DNAzyme-regulated CRISPR-Cas12a biosensor. The objects are not drawn in real scale. (B) A 1.5% agarose gel electrophoresis image of the proposed transduction pathway by trans-cleavage of ssDNA−FAM. Bands 1−5: ssDNA−FAM, ssDNA−FAM + Cas12a/CrRNA, ssDNA−FAM + Cas12a/CrRNA + locked activator, ssDNA−FAM + Cas12a/CrRNA + locked activator + Na^+, ssDNA−FAM + Cas12a/CrRNA + pure activator. (C) Persistent luminescence spectra of the proposed transduction pathway by the trans-cleavage reporters-coupled LPN. Lines 1−5: reporters-coupled LPN, Cas12a/CrRNA + reporters-coupled LPN, Cas12a/CrRNA + reporters-coupled LPN + locked activator, Cas12a/CrRNA + reporters-coupled LPN + locked activator + Na^+, Cas12a/CrRNA + reporters-coupled LPN + pure activator. (D) Persistent luminescence images (false-color) on PDMS (bottom) and PC (top) films in the presence of different amounts of Na^+ (from 80 nM to 5000 μM). (E) Investigation of the linear working curves between the relative luminescence intensity and the logarithm of $[Na^+]$ on PDMS and PC films, respectively. (F) Specificity of the Na^+ measurement toward metal cations from monovalent to trivalent, NH_4^+, BSA, DNA, and RNA. Concentrations of these substances are 10-fold higher than that of Na^+. ***$P < 0.001$; **$P < 0.01$; ns, no significant difference ($P > 0.05$).

gel electrophoresis (Figure 3B) and luminescence study (Figure 3C). For the former, the CEA-activated CRISPR-Cas12a system can effectively cleave a random FAM-labeled single-stranded DNA substrate (ssDNA−FAM) into a series of short fragments, and such a degradation process is very similar to that of the presence of pure activator, whereas a completely silent manner appears in the absence of CEA. For the latter, the comparison of signal intensities attests that the inactive case cannot make the quenched persistent luminescence recover, while a considerable signal recovery sign is detected for the CEA-introduced group.

After choosing the optimal collateral cleavage conditions on the LPN surface (Figure S11), i.e., the temperature, pH, and time are 37 °C, 8.0, and 15 min, respectively, and performing the time-gated luminescence readout (10 s after removing the excitation source) under different amounts of CEA, it gives a trend that the brightness of the chip holes on the PC film greatly relies on the concentration of CEA (Figure 3D, top image), implying that the increasing targets can be in favor of a more pronounced recovery phenomenon for the persistent luminescence. In contrast, due to the lack of effective signal amplification, very weak luminescence signals are exhibited on the PDMS film within the same concentration range (Figure 3D, bottom image). By further making use of an ImageJ software to quantify these false-color images, it also comes to follow that the PC film can result in a strict linear working curve (R^2: 0.9925, Figure 3E) crossing up to 5 orders of magnitude (from 5 pg/mL to 200 ng/mL) between the relative luminescence intensity $[(I - I_0)/I_0$, where I and I_0 indicate the luminescence signals with and without the introduction of CEA, respectively] and the logarithm of [CEA]. According to the calculation criterion (3σ/slope, where σ represents the standard deviation derived from seven parallel measurements of blank sample), an ultrasensitive analysis performance with a limit of detection (LOD) down to 3.6 pg/mL is acquired. Such an outstanding LOD is not only significantly lower than that of the traditional CEA kit (e.g., chemiluminescence immunoassay ~0.5 ng/mL) but also shows a potent competitiveness toward other advanced optical sensing methods (Table S1).

Having investigated the sensitivity, another momentous concern is specificity because potential interfering matrixes exist generally in human body fluids. For this reason, the constructed CRISPR-Cas12a biosensor is utilized to respond to four analogous proteins (BSA, AFP, PSA, and IgG) and three plasma proteins (albumin, globulins, and fibrinogen), other biomolecules (DNA and RNA), and some small molecules (Na^+ and K^+). The evaluation results are presented in Figure 3F, among which the introduction of CEA produces the most conspicuous luminescence intensity ($P < 0.001$). On account of the high selectivity of the aptamer, the selected analogues and the representative plasma substances can make only fairly little contributions to the recovered luminescence even at very high concentrations (10-fold higher than that of CEA, $P < 0.05$), and those signals occupy only 6−8% against the CEA group. Furthermore, in consideration of the impossible binding event for the completely nonspecific substances, neither the nucleic acids nor the trace metal ions are able to generate signals that are overtly different from the blank group ($P > 0.05$). Overall, our method has superior specificity to face with the forthcoming detection of complicated sample.

https://doi.org/10.1021/acs.analchem.1c01403
Anal. Chem. 2021, 93, 12514−12523

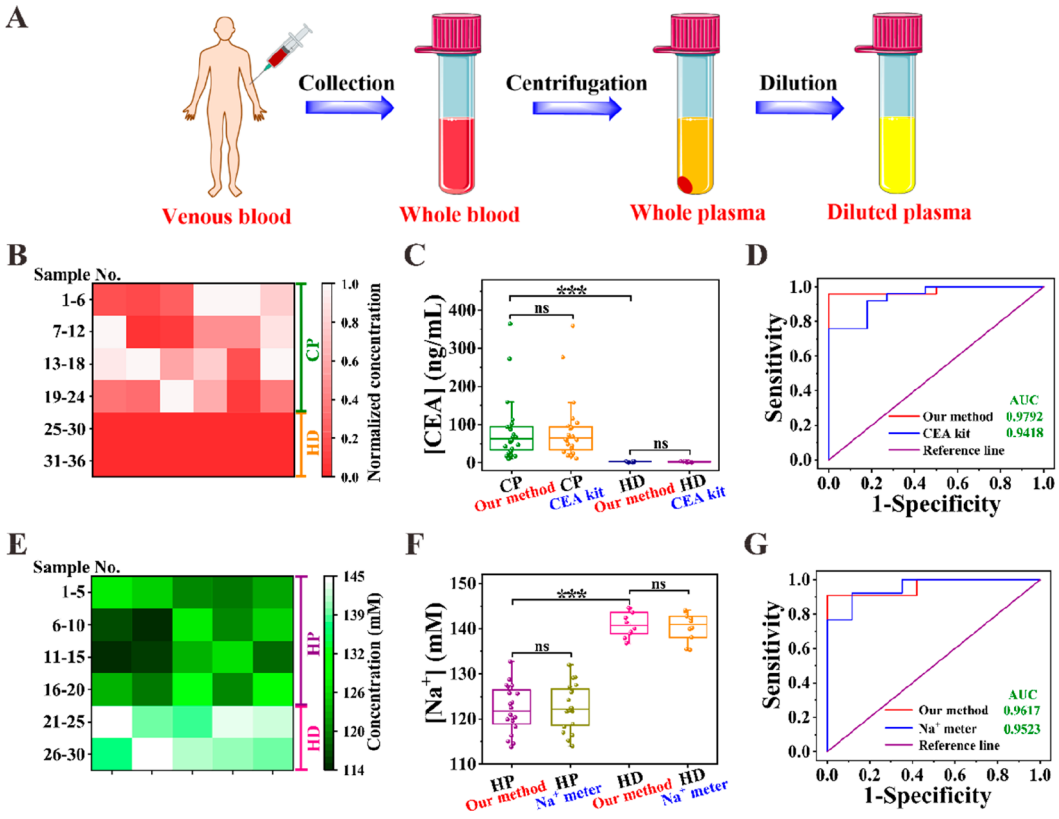

Figure 5. (A) Pretreatment steps of human blood samples. The objects are not drawn in real scale. (B) Heat map of the CEA content in CPs (24 cases) and HDs (12 cases) using our method. (C) Comparison between our method and a CEA kit. (D) ROC curves of our method and a CEA kit. (E) Heat map of the Na^+ levels in HPs (20 cases) and HD (10 cases) using our method. (F) Comparison between our method and a Na^+ meter. (G) ROC curves of our method and a Na^+ meter. ***$P < 0.001$; ns, no significant difference ($P > 0.05$).

Principle of the DNAzyme-Regulated CRISPR-Cas12a Biosensor and Its Analysis Performance toward Standard Na^+. Encouraged by the results of the CEA analysis, the fDNA-initiated regulation concept is next expanded to quantitatively measure Na^+ to examine its universality. In our design, a currently discovered Na^+-driven DNAzyme[38] possessing the function of enzyme catalysis is employed as an alternative fDNA (Figure 4A). Particularly, an annealing operation is first conducted to actualize the complementation between the two binding arms of the DNAzyme and the activator embedded into a substrate chain to fulfill a locking effect. In the presence of Na^+, the loop structure of the DNAzyme will specifically incorporate this cofactor, and then initiate an efficient RNA cleavage reaction at the rA position (the optimal reaction conditions are presented in Figure S12). Since the melting temperature (26 °C) for the hybridized right binding arm is much lower than the incubation circumstance (37 °C), the free combination of the released activator and a Cas12a/CrRNA complex is finally realized to activate the CRISPR-Cas12a system. Like the CEA sensing, the above flexible transduction pattern is ascertained successively by the visible discrepancies that emerge in electrophoresis image (Figure 4B) and luminescence spectra (Figure 4C). Following the same verification process for the analysis performance, the target concentration dependent luminescence recovery manner (Figure 4D) can be also attributed to a wide linear relationship (R^2: 0.9973, Figure 4E) ranging from 80 nM to 5000 μM, and the LOD is estimated to be as low as 63 nM (which is slightly higher than our previous work[21] due to the different signal collectors), exhibiting an apparent sensitivity advantage over the frequently used Na^+ meter (LOD ∼ 10 μM) and the recently reported optical biosensors (Table S2). More than that, profiting from the specific identification of the metal ions driven DNAzyme, the analytical methodology can hardly respond to other nonspecific metal cations from monovalent to trivalent or a representative nonmetallic cation as well as some biomacromolecules (Figure 4F).

Sensing Ability in Human Plasma Samples. In clinical practice, CEA is a kind of broad-spectrum tumor biomarker, and it plays an important role in the development and progression of various cancers such as rectal and gastric cancers.[39−41] Meanwhile, Na^+ is the most fundamental inorganic element primarily participating the water metabolism in many sorts of body fluids to hold the balance for a range of physiological parameters (e.g., pH and osmotic pressure),[42−44] and there will be diverse symptoms including asthenia and headache if this trace ion is massively lacking ($[Na^+] < 135$ mM). Therefore, establishing a sensitive and accurate biosensor to determine these targets in real samples is of great urgency in laboratory medicine. To this end, the assay approach is finally exploited for response in human plasma samples.

With regard to the underlying background interference (particularly autoluminescence) originating from such a complicated biological medium, it is necessary to go over the adaptability before accomplishing the proposed task. Satisfactorily, benefiting from the merit of persistent luminescence, the serious autoluminescence signals in whole plasma under 365 nm UV excitation are entirely overcome (Figure S13A), and no evident fluctuations appear to the signal-to-background ratios

https://doi.org/10.1021/acs.analchem.1c01403
Anal. Chem. 2021, 93, 12514−12523

(on the PC films) for this challenging medium (Figure S13B), expressing a strong anti-interference feature to ensure the reliability of the acquired optical information. After performing centrifugation to the collected venous bloods from corresponding patients and healthy donors, the yellow plasmas are diluted thoroughly to allow the measured signals fall into the as-obtained linear scope (Figure 5A).

The heat map (Figure 5B) clearly shows the definite CEA contents in cancer patients (CPs, 24 cases) with abnormal CEA expressions and healthy donors (HDs, 12 cases), and their values are basically in accordance with those analyzed by a CEA kit using chemiluminescence (Figure 5C, $P > 0.05$). Moreover, good accuracy is certified by receiver operating characteristic (ROC) curves (Figure 5D), under which the area under the curve (AUC) data are as high as 0.9792 and 0.9418 for our method and the CEA kit, respectively. Similarly, the different Na^+ levels in hyponatremia patients (HPs, 20 cases) and HDs (10 cases) can be effectively distinguished (Figure 5E), and the results unfold no significant difference to the traditional Na^+ meter (Figure 5F, $P > 0.05$). Also, the accuracy of our method is compared to this gold-standard test (Figure 5G, AUCs data are 0.9617 and 0.9523, respectively). Together, these clinical attempts demonstrate a certain application prospect for the newly developed biosensors.

CONCLUSIONS

This work has highlighted a meaningful luminescent CRISPR-Cas12a biosensor. By virtue of the extensive target recognition of fDNA, the biosensors perform with a "lock-to-activator" switching mode, and they can be effectively applied to transduce a protein (CEA) and a metal ion (Na^+) by employing dual aptamers and DNAzyme, respectively. Moreover, the working ability in complicated biological samples is significantly improved by using an attractive LPN-supported time-gated imaging strategy to perfectly avoid the background autofluorescence. To prevent the decay of persistent luminescence and realize signal amplification, a portable PC film formed biomimetic periodic chip is further fabricated to serve as the luminescence acquisition phase, resulting in an enhancement factor of up to 24.2-fold. After designing a simple "off-to-on" based LRET sensing strategy for the persistent luminescence signal, our assay approach is endowed with an ultrasensitive performance, wherein the LODs toward CEA and Na^+ are severally lowered to 3.6 pg/mL and 63 nM with outstanding specificity. Most importantly, this new analytical tool can enable the accurate clinical diagnosis of human plasma samples, demonstrating a favorable application prospect.

ASSOCIATED CONTENT

Supporting Information

The Supporting Information is available free of charge at https://pubs.acs.org/doi/10.1021/acs.analchem.1c01403.

Chemical reagents and materials, human blood samples, instrumentation, calculation of coupling number, analysis procedures of standard CEA and Na^+ in buffer solutions, specificity investigations for CEA and Na^+ analyses, analysis procedures of standard CEA and Na^+ in human plasma samples, size distributions of the LPN and LPN−NH_2, high-resolution TEM images of the LPN and LPN−NH_2, real digital images of the LPN and LPN−NH_2 solutions, dynamic light scattering data including ζ-potentials and hydrate particle sizes of the LPN and LPN−NH_2, demonstration of the coupling reaction, SEM image of the PC film after solution incubation, investigation of inter- and intrabatches of PC films, optimization results, investigation of background signals in human plasma, and assay performance comparisons (PDF)

AUTHOR INFORMATION

Corresponding Authors

Cheng-Yu Li − *School of Public Health, Medical College, Wuhan University of Science and Technology, Wuhan 430065, People's Republic of China;* orcid.org/0000-0003-4463-717X; Email: li-chengyu@wust.edu.cn

Hong-Wu Tang − *College of Chemistry and Molecular Sciences, Wuhan University, Wuhan 430072, People's Republic of China;* orcid.org/0000-0002-2258-6992; Email: hwtang@whu.edu.cn

Authors

Bei Zheng − *College of Chemistry and Molecular Sciences, Wuhan University, Wuhan 430072, People's Republic of China; School of Life Sciences, Westlake University, Hangzhou 310024, People's Republic of China*

Li-Li Lu − *School of Public Health, Medical College and Institute of Pharmaceutical Innovation, Medical College, Wuhan University of Science and Technology, Wuhan 430065, People's Republic of China*

Wen-Kai Fang − *College of Chemistry and Molecular Sciences, Wuhan University, Wuhan 430072, People's Republic of China*

Ming-Qiu Zheng − *College of Chemistry and Molecular Sciences, Wuhan University, Wuhan 430072, People's Republic of China*

Jia-Ling Gao − *School of Public Health, Medical College, Wuhan University of Science and Technology, Wuhan 430065, People's Republic of China*

Liu Yuheng − *School of Public Health, Medical College, Wuhan University of Science and Technology, Wuhan 430065, People's Republic of China*

Dai-Wen Pang − *College of Chemistry, Nankai University, Tianjin 300071, People's Republic of China;* orcid.org/0000-0002-7017-5725

Complete contact information is available at: https://pubs.acs.org/10.1021/acs.analchem.1c01403

Author Contributions

#C.-Y.L., B.Z., and L.-L.L. contributed equally to this work.

Notes

The authors declare no competing financial interest.

ACKNOWLEDGMENTS

This work was supported by the National Natural Science Foundation of China (21904102, 21827808, 81772256, and 81700446).

REFERENCES

(1) Li, H.; Steckl, A. J. *Anal. Chem.* **2019**, *91*, 352−371.

(2) Swiner, D. J.; Jackson, S.; Burris, B. J.; Badu-Tawiah, A. K. *Anal. Chem.* **2020**, *92*, 183−202.

(3) Jones, A.; Dhanapala, L.; Kankanamage, R. N. T.; Kumar, C. V.; Rusling, J. F. *Anal. Chem.* **2020**, *92*, 345−362.

(4) Ma, C.; Cao, Y.; Gou, X. D.; Zhu, J. J. *Anal. Chem.* **2020**, *92*, 431−454.

(5) Horvath, P.; Barrangou, R. *Science* **2010**, *327*, 167−170.
(6) Wang, X. S.; Xiong, E. H.; Tian, T.; Cheng, M.; Lin, W.; Wang, H.; Zhang, G. H.; Sun, J.; Zhou, X. M. *ACS Nano* **2020**, *14*, 2497−2508.
(7) Yuan, C. Q.; Tian, T.; Sun, J.; Hu, M. L.; Wang, X. S.; Xiong, E. H.; Cheng, M.; Bao, Y. J.; Lin, W.; Jiang, J. M.; Yang, C. W.; Chen, Q.; Zhang, H.; Wang, H.; Wang, X. R.; Deng, X. B.; Liao, X. P.; Liu, Y. H.; Wang, Z.; Zhang, G. H.; Zhou, X. M. *Anal. Chem.* **2020**, *92*, 4029−4037.
(8) Hu, M. L.; Yuan, C. Q.; Tian, T.; Wang, X. S.; Sun, J.; Xiong, E. H.; Zhou, X. M. *J. Am. Chem. Soc.* **2020**, *142*, 7506−7513.
(9) Chen, X. L.; Cao, G. H.; Zhang, J. J.; Deng, Y. Y.; Luo, X. G.; Yang, M.; Huo, D. Q.; Hou, C. J. *Sens. Actuators, B* **2021**, *333*, 129553.
(10) Dai, Y. F.; Somoza, R. A.; Wang, L.; Welter, J. F.; Li, Y.; Caplan, A. I.; Liu, C. C. *Angew. Chem., Int. Ed.* **2019**, *58*, 17399−17405.
(11) Zhang, D. C.; Yan, Y. R.; Que, H. Y.; Yang, T. T.; Cheng, X. X.; Ding, S. J.; Zhang, X. M.; Cheng, W. *ACS Sensors* **2020**, *5*, 557−562.
(12) Xu, W.; Jin, T.; Dai, Y. F.; Liu, C. C. *Biosens. Bioelectron.* **2020**, *155*, 112100.
(13) Shan, Y. Y.; Zhou, X. M.; Huang, R.; Xing, D. *Anal. Chem.* **2019**, *91*, 5278−5285.
(14) Liang, M. D.; Li, Z. L.; Wang, W. S.; Liu, J. K.; Liu, L. S.; Zhu, G. L.; Karthik, L.; Wang, M.; Wang, K. F.; Wang, Z.; et al. *Nat. Commun.* **2019**, *10*, 3672.
(15) Wang, D. X.; Wang, J.; Du, Y. C.; Ma, J. Y.; Wang, S. Y.; Tang, A. N.; Kong, D. M. *Biosens. Bioelectron.* **2020**, *168*, 112556.
(16) Xiong, Y.; Zhang, J. J.; Yang, Z. L.; Mou, Q. B.; Ma, Y.; Xiong, Y. H.; Lu, Y. *J. Am. Chem. Soc.* **2020**, *142*, 207−213.
(17) Chen, Q.; Tian, T.; Xiong, E. H.; Wang, P.; Zhou, X. M. *Anal. Chem.* **2020**, *92*, 573−577.
(18) Li, H.; Li, M. L.; Yang, Y. C.; Wang, F.; Wang, F.; Li, C. *Anal. Chem.* **2021**, *93*, 3209−3216.
(19) Chen, J. S.; Ma, E. B.; Harrington, L. B.; Da Costa, M.; Tian, X. R.; Palefsky, J. M.; Doudna, J. A. *Science* **2018**, *360*, 436−439.
(20) Gootenberg, J. S.; Abudayyeh, O. O.; Kellner, M. J.; Joung, J.; Collins, J. J.; Zhang, F. *Science* **2018**, *360*, 439−444.
(21) Li, C. Y.; Kang, Y. F.; Qi, C. B.; Zheng, B.; Zheng, M. Q.; Song, C. Y.; Guo, Z. Z.; Lin, Y.; Pang, D. W.; Tang, H. W. *Anal. Chem.* **2019**, *91*, 7950−7957.
(22) Li, C. Y.; Zhang, T.; Kang, Y. F.; Qi, C. B.; Zheng, B.; Xu, C. M.; Lin, Y.; Pang, D. W.; Tang, H. W. *Chem. Commun.* **2020**, *56*, 6997−7000.
(23) Li, C. Y.; Zheng, B.; Li, J. T.; Gao, J. L.; Liu, Y. H.; Pang, D. W.; Tang, H. W. *ACS Nano* **2021**, *15*, 8142−8154.
(24) Fu, X. Y.; Liu, C. L.; Shi, J. P.; Man, H. Z.; Xu, J.; Zhang, H. W. *Opt. Mater.* **2014**, *36*, 1792−1797.
(25) Wang, J.; Ma, Q. Q.; Liu, H. Y.; Wang, Y. Q.; Shen, H. J.; Hu, X. X.; Ma, C.; Yuan, Q.; Tan, W. H. *Anal. Chem.* **2017**, *89*, 12764−12770.
(26) Wang, J.; Ma, Q. Q.; Zheng, W.; Liu, H. Y.; Yin, C. Q.; Wang, F. B.; Chen, X. Y.; Yuan, Q.; Tan, W. H. *ACS Nano* **2017**, *11*, 8185−8191.
(27) Wang, Y. Q.; Li, Z. H.; Lin, Q. S.; Wei, Y. R.; Wang, J.; Li, Y. X.; Yang, R. H.; Yuan, Q. *ACS Sensors* **2019**, *4*, 2124−2130.
(28) Wang, B. B.; Zhao, X.; Chen, L. J.; Yang, C.; Yan, X. P. *Anal. Chem.* **2021**, *93*, 2589−2595.
(29) Potyrailo, R. A.; Bonam, R. K.; Hartley, J. G.; Starkey, T. A.; Vukusic, P.; Vasudev, M.; Bunning, T.; Naik, R. R.; Tang, Z. X.; Palacios, M. A.; Larsen, M.; Le Tarte, L. A.; Grande, J. C.; Zhong, S.; Deng, T. *Nat. Commun.* **2015**, *6*, 7959.
(30) Hou, J.; Zhang, H. C.; Yang, Q.; Li, M. Z.; Song, Y. L.; Jiang, L. *Angew. Chem., Int. Ed.* **2014**, *53*, 5791−5795.
(31) Min, K.; Choi, S.; Choi, Y.; Jeon, H. *Nanoscale* **2014**, *6*, 14531−14537.
(32) Yao, Q.; Wang, Y. Q.; Wang, J.; Chen, S. M.; Liu, H. Y.; Jiang, Z. R.; Zhang, X. E.; Liu, S. M.; Yuan, Q.; Zhou, X. *ACS Nano* **2018**, *12*, 6777−6783.
(33) Li, Q.; Zhou, S. H.; Zhang, T.; Zheng, B.; Tang, H. W. *Biosens. Bioelectron.* **2020**, *150*, 111866.
(34) Li, Y.; Gecevicius, M.; Qiu, J. R. *Chem. Soc. Rev.* **2016**, *45*, 2090−2136.
(35) Gutiérrez Moreno, J. J.; Pan, K.; Wang, Y.; Li, W. J. *Langmuir* **2020**, *36*, 5680−5689.
(36) Gabelica, V.; Rosu, F.; Tabarin, T.; Kinet, C.; Antoine, R.; Broyer, M.; De Pauw, E.; Dugourd, P. *J. Am. Chem. Soc.* **2007**, *129*, 4706−4713.
(37) Lin, X. J.; Li, S. Q.; Zhang, B. G.; Yang, H.; Zhang, K.; Huang, H. G. *Anal. Methods* **2020**, *12*, 5496−5502.
(38) Chen, K.; Huang, Q.; Fu, T.; Ke, G. L.; Zhao, Z. B.; Zhang, X. B.; Tan, W. H. *Anal. Chem.* **2020**, *92*, 7404−7408.
(39) Fletcher, R. H. *Ann. Intern. Med.* **1986**, *104*, 66−73.
(40) van Manen, L.; Groen, J. V.; Putter, H.; Pichler, M.; Vahrmeijer, A. L.; Bonsing, B. A.; Mieog, J. S. D. *Cancers* **2020**, *12*, 2970.
(41) Wu, Q.; Li, N. B.; Wang, Y.; Xu, Y. C.; Wu, J. D.; Jia, G. R.; Ji, F. J.; Fang, X. D.; Chen, F. F.; Cui, X. Q. *Anal. Chem.* **2020**, *92*, 3354−3360.
(42) Simpson, F. O. *Lancet* **1988**, *332*, 25−29.
(43) Scotney, B.; Reid, S. *Clin J. Sport Med.* **2015**, *25*, 341−346.
(44) Megahed, A. A.; Hiew, M.; Grunberg, W.; Trefz, F. M.; Constable, P. D. *J. Dairy Sci.* **2019**, *102*, 7435−7444.

https://doi.org/10.1021/acs.analchem.1c01403
Anal. Chem. 2021, 93, 12514−12523